

# Vacuum Beam Guide for Large Scale Quantum Networks

Yuexun Huang,<sup>1,\*</sup> Francisco Salces – Carcoba,<sup>2</sup> Rana X Adhikari,<sup>2</sup> Amir H. Safavi-Naeini,<sup>3</sup> and Liang Jiang<sup>1,†</sup>

<sup>1</sup>*Pritzker School of Molecular Engineering, University of Chicago, Chicago, Illinois 60637, USA*

<sup>2</sup>*Division of Physics, Math, and Astronomy, LIGO Laboratory,  
California Institute of Technology, Pasadena, CA 91125 USA*

<sup>3</sup>*Department of Applied Physics and Ginzton Laboratory, Stanford University, Stanford, CA 94305 USA*

(Dated: December 18, 2023)

The vacuum beam guide (VBG) presents a completely different solution for quantum channels to overcome the limitations of existing fiber and satellite technologies for long-distance quantum communication. With an array of aligned lenses spaced kilometers apart, the VBG offers ultra-high transparency over a wide range of optical wavelengths. With realistic parameters, the VBG can outperform the best fiber by three orders of magnitude in terms of attenuation rate. Consequently, the VBG can enable long-range quantum communication over thousands of kilometers with quantum channel capacity beyond  $10^{13}$  qubit/sec, orders of magnitude higher than the state-of-the-art quantum satellite communication rate. Remarkably, without relying on quantum repeaters, the VBG can provide a ground-based, low-loss, high-bandwidth quantum channel that enables novel distributed quantum information applications for computing, communication, and sensing.

It is an outstanding challenge to build an effective low-loss quantum channel for global-scale quantum networks, which will enable transformative applications of secure quantum communication [1], distributed quantum sensing [2], and network-based quantum computation [3, 4]. The main obstacle is the absorption loss of optical channels, with attenuation length limited to tens of kilometers for fiber and free-space channels, resulting in an exponential decrease in the direct quantum communication rate over long distances. Significant progress has been made in extending the communication distances for quantum networks, including satellite-based quantum entanglement distribution over 1200 km [5] and memory-enhanced quantum communication [6] beyond the repeater-less bound [7, 8]. However, satellite-based quantum channels are fragile, expensive, and restricted by local weather conditions [9]. Furthermore, quantum repeaters without full quantum error correction will still suffer from a polynomial decrease in communication rate over long distances [10]. Hence, it is highly desirable to establish a reliable quantum channel capable of directly transmitting quantum signals over vast distances, such as the continental scale of  $10^4$  km (with an attenuation rate of at the level of  $10^{-4}$  dB/km) for a wide range of optical frequencies.

To overcome this challenge, we explore a completely different approach – the vacuum beam guide (VBG) – which uses an array of lenses (in an evacuated tube) to guide light, as opposed to relying on total reflection induced by fiber. The large vacuum spacing between lenses significantly reduces the effective travel length of light in optical materials, thus eliminating the problem of material absorption. Inspired by quantum communication satellites, the VBG channel is set up within a vacuum

chamber tube, which eliminates air absorption and effectively isolates the channel from the outer environment, ensuring robustness against environmental perturbations. Although beam waveguides were proposed for classical optical communication [11], it was taken over by low-cost optical fiber, which is sufficient for classical communication, despite its intrinsic loss. For quantum communication, however, it is crucial that the design of the vacuum beam guide has the potential to achieve ultra-low-loss long-distance communication. With the ability to build large-scale vacuum chambers hosting precision optical elements separated by multiple kilometers, we can make exciting scientific discoveries, such as gravitational wave detection by the Laser Interferometer Gravitational-wave Observatory (LIGO) [12].

Here, we propose deploying the VBG as the backbone quantum channel toward a global quantum network with a hierarchy structure as shown in Fig. 1(a-b). We model the system and estimate the upper bound of the attenuation dominated by residue air absorption, optical losses introduced by lenses, and misalignment of the beam guide. Our estimation demonstrates the VBG as state-of-the-art under a practical and exemplifying configuration, establishing it as one of the most practical and potentially useful quantum communication techniques at a global scale.

*Ultra-High Transmission of VBG.* The VBG is a long vacuum chamber tube that consists of an array of  $N_{\text{tot}}$  lenses spaced  $L_0$  apart, which enables the connection of quantum terminals separated by  $L_{\text{tot}} = N_{\text{tot}}L_0$ , as illustrated in Fig. 1(c). The vacuum has a typical pressure below  $\sim 1$  Pascal, which ensures low absorption from the remaining gas at room temperature. The lenses are shielded from seismic vibrations and are optically aligned with adaptive feedback. In this analysis, we consider a feasible and robust confocal design with a spacing of  $L_0 = 4$  km and a focal length of  $f = L_0/2$ . The beam waist is  $w_0 = \sqrt{\lambda f/\pi} \approx 3$  cm for the telecom-band wavelength  $\lambda$ . The lens radius of  $R = 10$  cm is sufficient to

\* [yesunhuang@uchicago.edu](mailto:yesunhuang@uchicago.edu)

† [liang.jiang@uchicago.edu](mailto:liang.jiang@uchicago.edu)

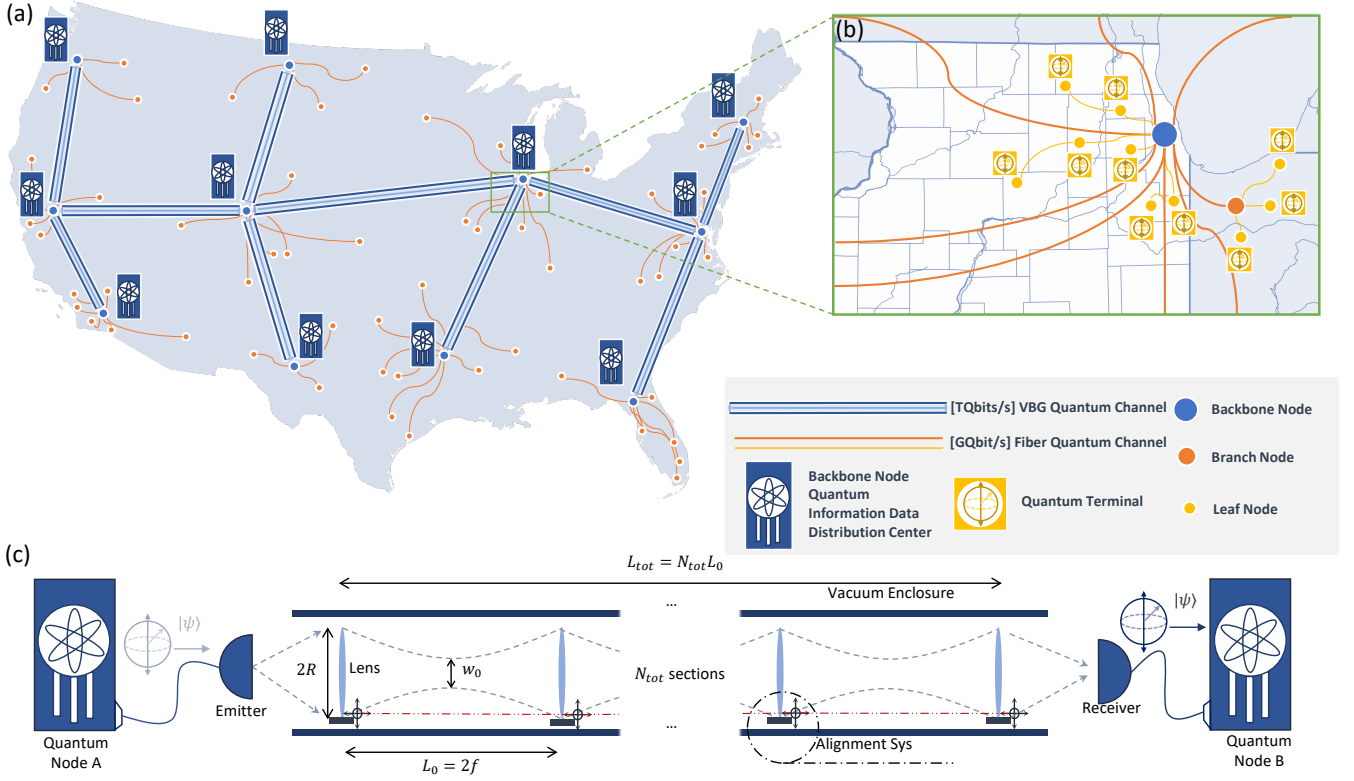


FIG. 1. A hierarchical structure of large-scale quantum networks connected by vacuum beam guides (VBGs). (a) The VBG backbone network (blue links) can transfer quantum information with high capacity (with TeraQubits/sec) over long distances, connecting regional quantum networks (orange links). (b) The regional network consists of fiber or free-space quantum channels designed to distribute quantum information to branch nodes and quantum terminals (with GigaQubits/sec) across urban scales. (c) The design of the VBG involves placing lenses with identical focus length  $f$  and radius  $R$  at regular intervals within a vacuum chamber tube, constructing a VBG with  $N_{tot}$  sections. The positions of the lenses are stabilized by an advanced alignment system. In the VBG, the fundamental Gaussian mode with waist  $w_0$  can travel at an extremely low loss over a distance of  $L_{tot}$ . Quantum states can be transferred from quantum node A at one end of the VBG to quantum node B at the other end of the VBG.

achieve negligible diffraction loss.

Optical signals encoding quantum information can transmit through the VBG with little loss, even after passing through an array of aligned lenses over thousands of kilometers. The effective attenuation rate (in units of dB/km) characterizes the VBG transmission loss, with three major contributions associated with the lens, residual gas, and imperfect alignment:

$$\alpha_{tot} = \alpha_{lens} + \alpha_{gas} + \alpha_{align}. \quad (1)$$

We now discuss the conditions to achieve an attenuation rate at the level of  $10^{-4}$  dB/km for all three contributions.

The lens loss,  $\alpha_{lens}$ , is associated with absorption, scattering, reflection, and diffraction. As illustrated in Fig. 2(a), a lens radius of  $R \geq 10$  cm is adequate to suppress diffraction loss for  $L_0 = 4$  km. Furthermore, by adding a multi-layer anti-reflective coating, the total loss per lens can be reduced to less than  $10^{-4}$ , resulting in an effective loss rate of  $\alpha_{lens} < 10^{-4}$  dB/km at the wavelengths  $\lambda \approx 1550$  nm, which can match the telecom band

(see Appendix A).

Gas loss in the VBG is primarily due to the absorption from residual air in the vacuum chamber tube. As shown in Fig. 2(b), we compute the attenuation rate  $\alpha_{gas}$  at various levels of gas pressure with the components of air based on the HITRAN database [15]. At a pressure of 1 Pascal, the attenuation rate is  $\alpha_{gas} < 10^{-4}$  dB/km for optical wavelengths within the selected telecom bands. Further reducing the air pressure below  $10^{-2}$  Pascal is sufficient to achieve negligible air absorption by reducing attenuation rate below  $10^{-4}$  dB/km almost over the entire spectrum.

We can derive an upper bound for the effective attenuation rate induced by imperfect alignment in the confocal design:

$$\alpha_{align} \leq -\frac{10}{L_0} \log_{10} \left[ 1 - \frac{2\sigma_s^2}{w_0^2} - \frac{\sigma_{L_0}^2}{L_0^2} - \frac{\sigma_f^2}{f^2} \right], \quad (2)$$

where  $\sigma_s$  and  $\sigma_{L_0}$  are the magnitudes of the fluctuations of transverse and longitudinal displacements for

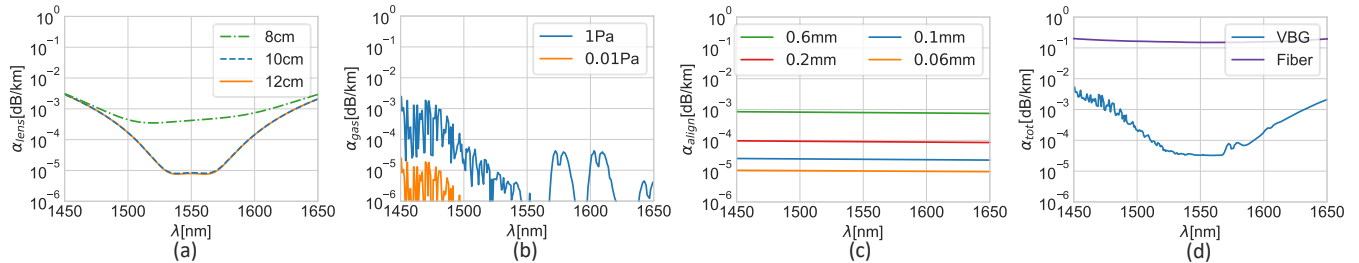


FIG. 2. Different effective attenuation rates as a function of wavelength under various configurations. (a) Attenuation rate from the lenses,  $\alpha_{\text{lens}}$ , with lens radius  $R = 8, 10, 20$  cm. For a large radius ( $R \geq 10$  cm), the lens loss is limited by residual reflection and absorption from the AR coating. (b) Attenuation rate due to residual gas,  $\alpha_{\text{gas}}$ , with moderate vacuum pressures:  $P = 0.01, 1$  Pa. (c) The misalignment attenuation rate,  $\alpha_{\text{align}}$ , with random transverse displacements  $\sigma_s = 0.06, 0.1, 0.2, 0.6$  mm while fixing  $\frac{\sigma_{L_0}}{L_0} = \frac{\sigma_f}{f} = 0.1\%$ . (d) The total attenuation rate of the VBG compared to the advanced fiber [13, 14] under the configuration of  $L_0 = 4$  km,  $R = 10$  cm,  $P = 1$  Pascal, and  $\sigma_s = 0.1$  mm.

each lens, and  $\sigma_f$  is the deviation of the focal length. The general bound for  $\alpha_{\text{align}}$  for near confocal design are derived in Appendix B. Since  $w_0 \ll L_0, f$ , the fluctuating transverse displacement is the dominant cause of attenuation, while the other two contributions can be sufficiently small,  $\frac{\sigma_{L_0}}{L_0}, \frac{\sigma_f}{f} < 10^{-3}$ , achievable with current technology (see Appendix C). As illustrated in Fig. 2(c), it is essential to have good transverse alignment (e.g.,  $\sigma_s < 0.2$  mm) to achieve a low effective attenuation rate ( $\alpha_{\text{align}} < 10^{-4}$  dB/km). Even with relatively poor alignment (e.g.,  $\sigma_s = 0.6$  mm), we can still achieve  $\alpha_{\text{align}} < 10^{-2}$  dB/km, which is much better than the attenuation rate of fiber by at least an order of magnitude. Practically, each lens will be actively positioned using slow actuators, based on standard alignment sensing systems [16], bringing the residual mis-centering to  $< 0.1$  mm.

By summing up all three contributions, we can plot the total attenuation rate along with the individual contributions in Fig. 2(d), assuming practical parameters such as  $R = 10$  cm,  $P = 1$  Pascal, and  $\sigma_s = 0.1$  mm. The VBG can achieve an attenuation level as low as  $5 \times 10^{-5}$  dB/km for an optimized choice of wavelength within the atmospheric window, which corresponds to an effective attenuation length of 80,000 km, more than three orders of magnitude better than state-of-the-art fiber technology.

*Quantum Channel Capacities of VBG.* We can use the VBG as a highly transparent bosonic quantum channel to transmit quantum information over long distances [17]. The VBG has a transmission efficiency at wavelength  $\lambda$

$$\eta[\lambda] = 10^{-0.1L_{\text{tot}}\alpha[\lambda]}, \quad (3)$$

which can be used for various quantum communication protocols. For one-way quantum communication (e.g., from Alice to Bob only), the one-way pure-loss capacity

for a single wave packet at a wavelength  $\lambda$  is given by

$$q_1[\lambda] = \max \left[ \log_2 \left( \frac{\eta[\lambda]}{1 - \eta[\lambda]} \right), 0 \right], \quad (4)$$

which vanishes for  $\eta[\lambda] \leq 1/2$ . If the pure-loss VBG channel is further assisted by two-way classical communication (between Alice and Bob), the corresponding two-way pure-loss capacity at a wavelength  $\lambda$  is

$$q_2[\lambda] = \log_2 \left( \frac{1}{1 - \eta[\lambda]} \right). \quad (5)$$

which is finite for all  $\eta[\lambda] > 0$ .

As shown in the insets of Fig. 3, the VBG can have a broad band with a large one-way or two-way channel capacity over long distances. In the low-loss regime with  $L_{\text{tot}} \ll 1/\alpha$ , efficient multi-mode encoding techniques can be used to approach the asymptotic scaling of one-way channel capacity [18].

We can calculate the frequency-integrated channel capacity, which provides the maximum transmission rate of quantum information, by integrating over the frequency [19]:

$$Q_{1(\text{or}2)} \equiv \int q_{1(\text{or}2)} d\nu = \int q_{1(\text{or}2)}[\lambda] \frac{c}{\lambda^2} d\lambda, \quad (6)$$

for one-way and two-way quantum communication protocols, respectively. The VBG has a significant advantage over other techniques, particularly due to its ultra-low attenuation rate over a wide range of wavelengths, leading to an extremely large quantum capacity exceeding  $10^{13}$  qubits/second over a distance of  $10^4$  km under one-way quantum communication protocol as shown in Fig. 3(a). While the estimation in Fig. 3(b) suggests that even with a baseline coupling loss as large as 50%, where the one-way protocol fails, it is still possible to achieve a Tera-level qubit rate via two-way protocols for continental scale communication. This points out a practically feasible pathway toward ultra-fast global quantum networks.

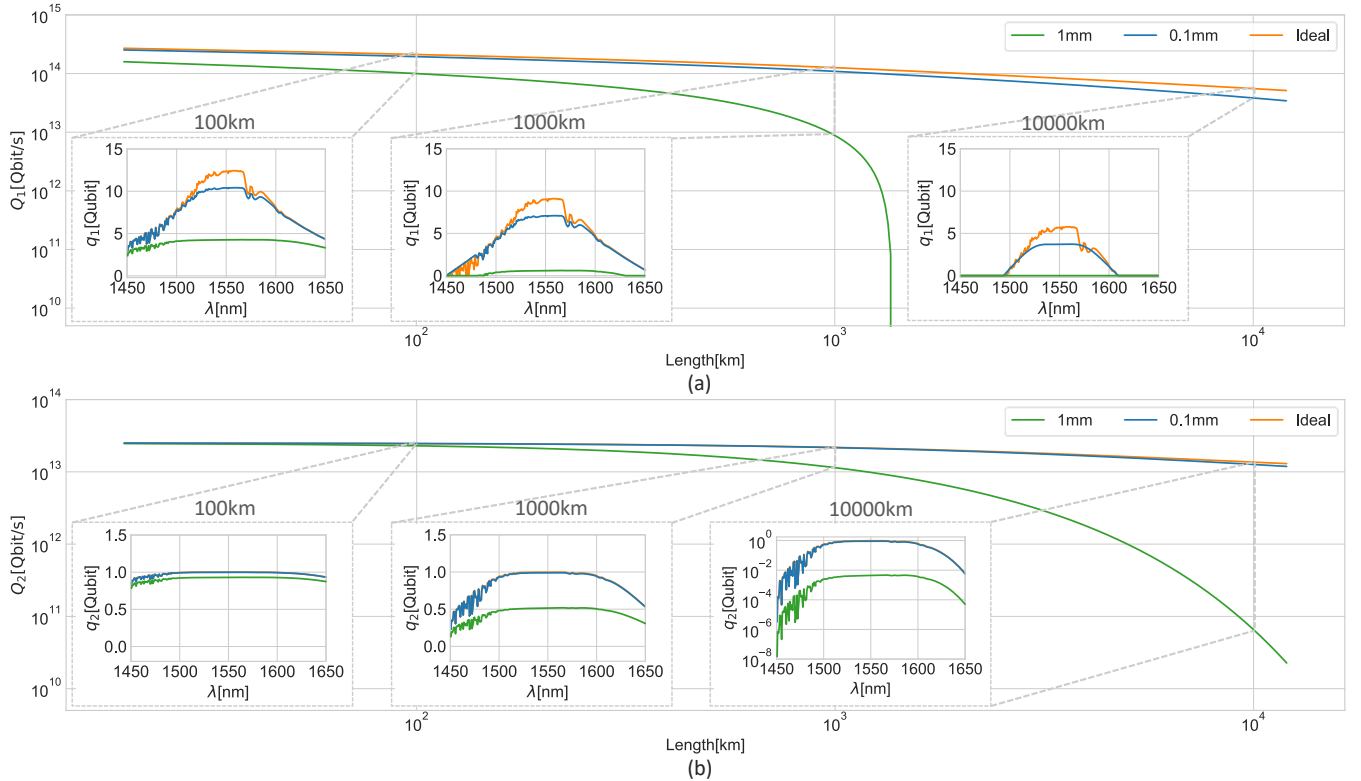


FIG. 3. The quantum channel capacity  $Q_{1(or_2)}$  at 1 Pascal as a function of transmission distance with  $\sigma_s = 0.1$ , 1 mm when fixing  $\frac{\sigma_{L_0}}{L_0} = \frac{\sigma_f}{f} = 0.1\%$  compared to the ideal alignment. (a) One-way frequency-integrated quantum capacity with perfect coupling. (b) Two-way frequency-integrated quantum capacity assuming 50% coupling efficiency. The insets show the relation between channel capacity  $q_{1(or_2)}$  as a function of wavelength at  $L = 100, 1000, 10000$  km. The inset of 10000 km in (b) is on log scale to show finite two-way quantum capacity over a wide range of parameters.

Compared to state-of-the-art satellite-ground links for quantum communication [20], the ground-based VBG offers high reliability as it is operational at all times, and provides an extremely high throughput, at least eight orders of magnitude higher in terms of achievable quantum communication rate. Additionally, unlike quantum repeaters [21], the VBG only requires passive optical lenses to focus the optical beams and does not need any quantum memory or active quantum devices to perform quantum error detection or correction. Therefore, the VBG should be feasible to implement with current technology.

*Discussion.* We can also design the VBG to operate with visible light, which would benefit from a larger air transmission window and low-loss lens materials if sufficiently small lens roughness is achievable, while better transversal alignment is required to match the reduced beam waist  $w_0 \propto \lambda^{1/2}$  with shorter wavelengths. In practice, there will be a trade-off between the VBG's performance and cost, and we can optimize its design parameters to achieve the desired balance.

*Summary and Outlook.* We have presented a ground-based VBG scheme that enables the implementation of a highly transparent and reliable optical quantum channel with an effective attenuation length of over  $10^4$  km

and a large communication bandwidth. With currently available technology, the VBG can establish a continuous quantum channel connecting remote quantum devices with an ultra-high quantum capacity above  $10^{13}$  qubits/second over continental scales, orders of magnitude higher than other approaches using satellites and quantum repeaters.

By addressing the challenge of lossy quantum channels, our high-throughput VBG has the potential to revolutionize quantum networks, enabling a wide range of exciting novel quantum network applications, such as global-scale secure quantum communication [1], ultra-long-based optical telescopes [2], quantum network of clocks [22], quantum data centers [23], and delegated quantum computing [24, 25].

*Acknowledgments* We thank David Awschalom, Saikat Guha, Dan Brown, Ming Lai, John Preskill and Peter Zoller for helpful comments and discussions. We acknowledge support from the ARO(W911NF-23-1-0077), ARO MURI (W911NF-21-1-0325), AFOSR MURI (FA9550-19-1-0399, FA9550-21-1-0209, FA9550-23-1-0338), NSF (PHY-0823459, PHY-1764464, ECCS-1941826, OMA-1936118, ERC-1941583, OMA-2137642, OSI-2326767, CCF-2312755), NTT Research, Packard

Foundation (2020-71479), and the Marshall and Arlene Bennett Family Research Program. This material is

based upon work supported by the U.S. Department of Energy, Office of Science, National Quantum Information Science Research Centers.

- 
- [1] F. Xu, X. Ma, Q. Zhang, H.-K. Lo, and J.-W. Pan, Secure quantum key distribution with realistic devices, *Reviews of Modern Physics* **92**, 025002 (2020).
- [2] D. Gottesman, T. Jennewein, and S. Croke, Longer-baseline telescopes using quantum repeaters, *Physical Review Letters* **109**, 070503 (2012).
- [3] H. J. Kimble, The quantum internet, *Nature* **453**, 1023 (2008).
- [4] S. Wehner, D. Elkouss, and R. Hanson, Quantum internet: A vision for the road ahead, *Science* **362**, eaam9288 (2018).
- [5] J. Yin, Y. Cao, Y.-H. Li, S.-K. Liao, L. Zhang, J.-G. Ren, W.-Q. Cai, W.-Y. Liu, B. Li, H. Dai, G.-B. Li, Q.-M. Lu, Y.-H. Gong, Y. Xu, S.-L. Li, F.-Z. Li, Y.-Y. Yin, Z.-Q. Jiang, M. Li, J.-J. Jia, G. Ren, D. He, Y.-L. Zhou, X.-X. Zhang, N. Wang, X. Chang, Z.-C. Zhu, N.-L. Liu, Y.-A. Chen, C.-Y. Lu, R. Shu, C.-Z. Peng, J.-Y. Wang, and J.-W. Pan, Satellite-based entanglement distribution over 1200 kilometers, *Science* **356**, 1140 (2017).
- [6] M. K. Bhaskar, R. Riedinger, B. Machielse, D. S. Levonian, C. T. Nguyen, E. N. Knall, H. Park, D. Englund, M. Lončar, D. D. Sukachev, and M. D. Lukin, Experimental demonstration of memory-enhanced quantum communication, *Nature* **580**, 60 (2020).
- [7] M. Takeoka, S. Guha, and M. M. Wilde, Fundamental rate-loss tradeoff for optical quantum key distribution, *Nat Commun* **5**, 10.1038/ncomms6235 (2014).
- [8] S. Pirandola, R. Laurenza, C. Ottaviani, and L. Banchi, The ultimate rate of quantum cryptography, *arXiv:1510.08863* (2015).
- [9] S.-K. Liao, W.-Q. Cai, W.-Y. Liu, L. Zhang, Y. Li, J.-G. Ren, J. Yin, Q. Shen, Y. Cao, Z.-P. Li, F.-Z. Li, X.-W. Chen, L.-H. Sun, J.-J. Jia, J.-C. Wu, X.-J. Jiang, J.-F. Wang, Y.-M. Huang, Q. Wang, Y.-L. Zhou, L. Deng, T. Xi, L. Ma, T. Hu, Q. Zhang, Y.-A. Chen, N.-L. Liu, X.-B. Wang, Z.-C. Zhu, C.-Y. Lu, R. Shu, C.-Z. Peng, J.-Y. Wang, and J.-W. Pan, Satellite-to-ground quantum key distribution, *Nature* **549**, 43 (2017).
- [10] S. Muralidharan, L. Li, J. Kim, N. Lütkenhaus, M. D. Lukin, and L. Jiang, Optimal architectures for long distance quantum communication, *Scientific Reports* **6**, 20463 (2016).
- [11] G. Goubau, Beam waveguides, *Advances in Microwaves* **3**, 67 (1968).
- [12] B. P. Abbott *et al.*, Observation of gravitational waves from a binary black hole merger, *Physical Review Letters* **116**, 061102 (2016).
- [13] M. Kakui, M. Matsui, T. Saitoh, and Y. Chigusa, Ultra-low-loss (0.1484 db/km) pure silica core fibre and extension of transmission distance, *Electronics Letters* **38**, 1 (2002).
- [14] H. Sakr, T. D. Bradley, G. T. Jasion, E. N. Fokoua, S. R. Sandoghchi, I. A. Davidson, A. Taranta, G. Guerra, W. Shere, Y. Chen, *et al.*, Hollow core nanfs with five nested tubes and record low loss at 850, 1060, 1300 and 1625nm, in *Optical Fiber Communication Conference* (Optica Publishing Group, 2021) pp. F3A–4.
- [15] R. V. Kochanov, I. Gordon, L. Rothman, P. Wcisło, C. Hill, and J. Wilzewski, Hitran application programming interface (hapi): A comprehensive approach to working with spectroscopic data, *Journal of Quantitative Spectroscopy and Radiative Transfer* **177**, 15 (2016).
- [16] K. L. Dooley, L. Barsotti, R. X. Adhikari, M. Evans, T. T. Fricke, P. Fritschel, V. Frolov, K. Kawabe, and N. Smith-Lefebvre, Angular control of optical cavities in a radiation-pressure-dominated regime: the enhanced ligo case, *J. Opt. Soc. Am. A* **30**, 2618 (2013).
- [17] A. S. Holevo and R. F. Werner, Evaluating capacities of bosonic gaussian channels, *Physical Review A* **63**, 032312 (2001).
- [18] K. Noh, V. V. Albert, and L. Jiang, Improved quantum capacity bounds of gaussian loss channels and achievable rates with gottesman-kitaev-preskill codes, *IEEE Transactions on Information Theory* **65**, 2563 (2019).
- [19] C.-H. Wang, F. Li, and L. Jiang, Quantum capacities of transducers, *Nature Communications* **13**, 6698 (2022).
- [20] Y.-A. Chen, Q. Zhang, T.-Y. Chen, W.-Q. Cai, S.-K. Liao, J. Zhang, K. Chen, J. Yin, J.-G. Ren, Z. Chen, S.-L. Han, Q. Yu, K. Liang, F. Zhou, X. Yuan, M.-S. Zhao, T.-Y. Wang, X. Jiang, L. Zhang, W.-Y. Liu, Y. Li, Q. Shen, Y. Cao, C.-Y. Lu, R. Shu, J.-Y. Wang, L. Li, N.-L. Liu, F. Xu, X.-B. Wang, C.-Z. Peng, and J.-W. Pan, An integrated space-to-ground quantum communication network over 4,600 kilometres, *Nature* **589**, 214 (2021).
- [21] K. Azuma, S. E. Economou, D. Elkouss, P. Hilaire, L. Jiang, H.-K. Lo, and I. Tzitrin, Quantum repeaters: From quantum networks to the quantum internet, *arXiv:2212.10820* (2022).
- [22] P. Komar, E. M. Kessler, M. Bishof, L. Jiang, A. S. Sorensen, J. Ye, and M. D. Lukin, A quantum network of clocks, *Nat Phys* **10**, 582 (2014).
- [23] J. Liu, C. T. Hann, and L. Jiang, Quantum data center: Theories and applications, *arXiv:2207.14336* (2022).
- [24] S. Barz, E. Kashefi, A. Broadbent, J. F. Fitzsimons, A. Zeilinger, and P. Walther, Demonstration of blind quantum computing, *science* **335**, 303 (2012).
- [25] J. F. Fitzsimons, Private quantum computation: an introduction to blind quantum computing and related protocols, *npj Quantum Information* **3**, 23 (2017).
- [26] J. C. Heurtley and W. Streifer, Optical resonator modes—circular reflectors of spherical curvature, *JOSA* **55**, 1472 (1965).
- [27] L. Pinard, B. Sassolas, R. Flaminio, D. Forest, A. Lacoudre, C. Michel, J. Montorio, and N. Morgado, Toward a new generation of low-loss mirrors for the advanced gravitational waves interferometers, *Optics letters* **36**, 1407 (2011).
- [28] R. Schnabel, M. Britzger, F. Brückner, O. Burmeister, K. Danzmann, J. Duck, T. Eberle, D. Friedrich, H. Luck, M. Mehmet, *et al.*, Building blocks for future detectors: Silicon test masses and 1550 nm laser light, in *Journal of Physics: Conference Series*, Vol. 228 (IOP Publishing,

- 2010) p. 012029.
- [29] M. H. Liyuan Zhang and G. Billingsley, Itm09 hr ar absorption, [LIGO Internal Document E1300674](#) (2013).
- [30] L. Pinard, C. Michel, B. Sassolas, L. Balzarini, J. Degallaix, V. Dolique, R. Flaminio, D. Forest, M. Granata, B. Lagrange, *et al.*, Mirrors used in the ligo interferometers for first detection of gravitational waves, *Applied optics* **56**, C11 (2017).
- [31] E. O. Inc, Anti-reflection(ar) coatings, <https://www.edmundoptics.com/knowledge-center/application-notes/lasers/anti-reflection-coatings/>.
- [32] A. Yariv and P. Yeh, *Photonics : optical electronics in modern communications*, 6th ed., The Oxford series in electrical and computer engineering (Oxford University Press, 2007).
- [33] G. Herzig and H. Weber, Equivalent optical resonators, *Applied Optics* **23**, 1450.1 (1984).
- [34] C. Eaglesfield, Mode-conversion loss in a sequential confocal lens system, in *Proceedings of the Institution of Electrical Engineers*, Vol. 111 (IET, 1964) pp. 610–615.
- [35] F. K. Schwering, On the theory of randomly misaligned beam waveguides, *IEEE Transactions on Microwave Theory and Techniques* **15**, 206 (1967).
- [36] W. H. Steier, The statistical effects of random variations in the components of a beam waveguide, *Bell System Technical Journal* **45**, 451 (1966).
- [37] J. Christian, G. Goubau, and J. Mink, 5.6-self-aligning optical beam waveguides+ c6553, *IEEE Journal of Quantum Electronics* **3**, 498 (1967).
- [38] W. Herrmannsfeldt, M. Lee, J. Spranza, and K. Trigger, Precision alignment using a system of large rectangular fresnel lenses, *Applied Optics* **7**, 995 (1968).
- [39] P. Fritschel, N. Mavalvala, D. Shoemaker, D. Sigg, M. Zucker, and G. González, Alignment of an interferometric gravitational wave detector, *Applied Optics* **37**, 6734 (1998).
- [40] S.-K. Liao, W.-Q. Cai, W.-Y. Liu, L. Zhang, Y. Li, J.-G. Ren, J. Yin, Q. Shen, Y. Cao, Z.-P. Li, *et al.*, Satellite-to-ground quantum key distribution, *Nature* **549**, 43 (2017).
- [41] A. K. Ekert, Quantum cryptography based on bell's theorem, *Physical review letters* **67**, 661 (1991).
- [42] C. H. Bennett and G. Brassard, Quantum cryptography: Public key distribution and coin tossing, *arXiv preprint arXiv:2003.06557* (2020).
- [43] A. S. Cacciapuoti, M. Caleffi, F. Tafuri, F. S. Cataliotti, S. Gherardini, and G. Bianchi, Quantum internet: networking challenges in distributed quantum computing, *IEEE Network* **34**, 137 (2019).
- [44] S.-J. Yang, X.-J. Wang, X.-H. Bao, and J.-W. Pan, An efficient quantum light–matter interface with sub-second lifetime, *Nature Photonics* **10**, 381 (2016).
- [45] L. Jiang, J. M. Taylor, K. Nemoto, W. J. Munro, R. Van Meter, and M. D. Lukin, Quantum repeater with encoding, *Physical Review A* **79**, 032325 (2009).
- [46] W. Dür, H.-J. Briegel, J. I. Cirac, and P. Zoller, Quantum repeaters based on entanglement purification, *Physical Review A* **59**, 169 (1999).
- [47] J. G. Rarity, P. Tapster, P. Gorman, and P. Knight, Ground to satellite secure key exchange using quantum cryptography, *New Journal of Physics* **4**, 82 (2002).
- [48] M. Aspelmeyer, H. R. Bohm, T. Gyatso, T. Jennewein, R. Kaltenbaek, M. Lindenthal, G. Molina-Terriza, A. Poppe, K. Resch, M. Taraba, *et al.*, Long-distance free-space distribution of quantum entanglement, *science* **301**, 621 (2003).
- [49] J. Yin, Y. Cao, Y.-H. Li, S.-K. Liao, L. Zhang, J.-G. Ren, W.-Q. Cai, W.-Y. Liu, B. Li, H. Dai, *et al.*, Satellite-based entanglement distribution over 1200 kilometers, *Science* **356**, 1140 (2017).
- [50] N. Gisin, G. Ribordy, W. Tittel, and H. Zbinden, Quantum cryptography, *Reviews of modern physics* **74**, 145 (2002).
- [51] W.-Y. Hwang, Quantum key distribution with high loss: toward global secure communication, *Physical review letters* **91**, 057901 (2003).
- [52] C.-Z. Peng, J. Zhang, D. Yang, W.-B. Gao, H.-X. Ma, H. Yin, H.-P. Zeng, T. Yang, X.-B. Wang, and J.-W. Pan, Experimental long-distance decoy-state quantum key distribution based on polarization encoding, *Physical review letters* **98**, 010505 (2007).
- [53] J. C. Palais, *Fiber optic communications*, Englewood Cliffs (1984).
- [54] B. Abbott, R. Abbott, R. Adhikari, P. Ajith, B. Allen, G. Allen, R. Amin, S. Anderson, W. Anderson, M. Arain, *et al.*, Ligo: the laser interferometer gravitational-wave observatory, *Reports on Progress in Physics* **72**, 076901 (2009).
- [55] S. Langenfeld, O. Morin, M. Körber, and G. Rempe, A network-ready random-access qubits memory, *npj Quantum Information* **6**, 86 (2020).
- [56] M. Pant, H. Krovi, D. Towsley, L. Tassiulas, L. Jiang, P. Basu, D. Englund, and S. Guha, Routing entanglement in the quantum internet, *npj Quantum Information* **5**, 25 (2019).
- [57] J. Liu, C. T. Hann, and L. Jiang, Quantum data center: Theories and applications, *arXiv preprint arXiv:2207.14336* (2022).
- [58] C. Weedbrook, S. Pirandola, R. García-Patrón, N. J. Cerf, T. C. Ralph, J. H. Shapiro, and S. Lloyd, Gaussian quantum information, *Reviews of Modern Physics* **84**, 621 (2012).
- [59] H. A. Macleod, *Thin-film optical filters* (CRC press, 2017).
- [60] I. H. Malitson, Interspecimen comparison of the refractive index of fused silica, *Josa* **55**, 1205 (1965).
- [61] M. J. Dodge, Refractive properties of magnesium fluoride, *Applied optics* **23**, 1980 (1984).
- [62] D. L. Wood and K. Nassau, Refractive index of cubic zirconia stabilized with yttria, *Applied Optics* **21**, 2978 (1982).

## Appendix A: Optical Losses due to the Lens Array

The major sources of optical loss (and thereby decoherence) in the VBG are due to the lens array. In the lens array, the major losses are  $l_{ab}$ , the absorption loss in the lens substrate as well as ARC coating,  $l_{sca}$ , the scattering loss from the lens surface (this includes scattering into low order Laguerre-Gauss modes that scatter back into the mean beam), and  $l_{ref}$ , the reflection loss due to the non-zero reflectivity of practical anti-reflection coatings (We assume here that reflected light has a random phase and does not interfere with the signal beam). Notice that we use a different quantity generally denoted by  $l$  to analyze the loss for convenience instead of using the effective attenuation rate  $\alpha$  used in the main text. They are related to each other by  $\alpha = -\frac{10}{L_0} \log(1-l)$ .

For a perfectly aligned confocal VBG with lenses of finite radius, the exact optical mode is described by the hyper-spheroidal function with a diffraction loss per section for rotation mode number  $m$  and radial mode number  $n$  in power ratio approximately given by: [26]

$$l_{d,nm} \approx \frac{\pi 2^{4n+2m+3} c^{2n+m+1} e^{-2c}}{\Gamma(n+1)\Gamma(n+m+1)}, \quad (\text{A1})$$

where  $c = \frac{kR^2}{L_0}$  is the Fresnel variable. Such a variable is assumed to be large enough ( $c \sim 10$ ) in this paper so that we can replace the hyper-spheroidal function with the Laguerre-Gauss function to describe the optical mode in the misalignment analysis. The total loss for the fundamental mode introduced by the lenses can be written as

$$l_{lens} = l_{d,00} + l_{ab} + l_{sca} + l_{ref}, \quad (\text{A2})$$

where approximate values for the losses are shown in Table I.

For a large enough radius ( $R \geq 10$  cm), lens loss is limited by residual ARC reflection and absorption. Commercially available telecom band ARC can achieve loss at the 100 ppm level, while our theoretical estimation shows that the ARC loss can be further improved to the 1 ppm level if we optimize the performance of a narrower transmission window, limited by the reflective loss of the ARC, as shown in the blue curve in Fig. 4(a). We will investigate the tradeoff between reflective loss and the transmission window of the ARC for better performance in future investigations.

Fig. 4(b) shows the one-way quantum capacity  $Q_1$  under different levels of lens loss. We observed that even with a 100-ppm level lens loss (red curve), it is still possible to achieve a non-zero communication rate over 10 thousand kilometers. Additionally, the maximum distance saturates when the lens loss reaches 1 ppm, with the performance mainly limited by misalignment.

TABLE I. The approximate values of different sources that contribute to the lens loss.

Sources	Values[ppm]
Lens diffraction, $l_{d,00}$	$10^{-4} \sim 2^\dagger$
Lens absorption, $l_{ab}$	$1 \sim 2$ [27–29]
Lens scattering, $l_{sca}$	$2.3 \sim 4.9$ [30]
Lens reflection, $l_{ref}$	$7 \sim 100^*$

<sup>†</sup>  $10^{-4}$  ppm is obtained by setting  $R = 12$ cm while 2 ppm is obtained by the default 10cm configuration.

\*100 ppm is rather pessimistic while commercially available [31]. And it can be further reduced to the level of a few ppm, as illustrated in Fig. 4(a) and measured in LIGO [30].

## Appendix B: Non-Confocal Design of VBG

Practically, it will be challenging for the VBG to fulfill the confocal condition over a wide range of wavelengths due to dispersion even using dispersion compensation. Fortunately, applying the well-known equivalent optical resonator method [32, 33], we can show that the non-confocal VBG fulfills the stability criteria,

$$\left(1 - \frac{L_0}{2f}\right)^2 < 1, \quad (\text{B1})$$

is uniquely equivalent to a confocal VBG with an equivalent focal length

$$f_{eq} = \sqrt{f_0(2f - f_0)}, f_0 = L_0/2 \quad (\text{B2})$$

and an equivalent Fresnel variable

$$c_{eq} = \frac{kR^2}{f_0(1/F + F)}, \quad (\text{B3})$$

where  $F = \frac{f_{eq}}{f_0}$ . The diffraction loss should now be calculated using Eq. A1 using the equivalent fresnel number. Let  $(r, \phi, z)$  denoted cylindrical coordinate along the VBG with the original point at the middle of the section, the field inside each section of VBG is thus given by

$$E_n^m(r, \phi, z) = E_0 \frac{w_0}{w(z)} e^{-\frac{r^2}{w^2(z)}} e^{-i(kz + \psi_0 + \frac{kr^2}{2R(z)} - \omega t)} \left(\frac{\sqrt{2}r}{w(z)}\right)^{|m|} L_n^{(|m|)}\left(\frac{2r^2}{w^2(z)}\right) e^{+i(|m|+2n+1)\psi} e^{-im\phi} \quad (\text{B4})$$

where

$$\psi = \arctan\left(\frac{z}{f_{eq}}\right), R(z) = z + \frac{f_{eq}^2}{z} \\ w_0 = \sqrt{\frac{2f_{eq}}{k}}, w(z) = w_0 \sqrt{1 + \frac{z^2}{f_{eq}^2}}, \quad (\text{B5})$$

which provides the fundamental mathematical description for the analysis of VBG in this paper. We can now

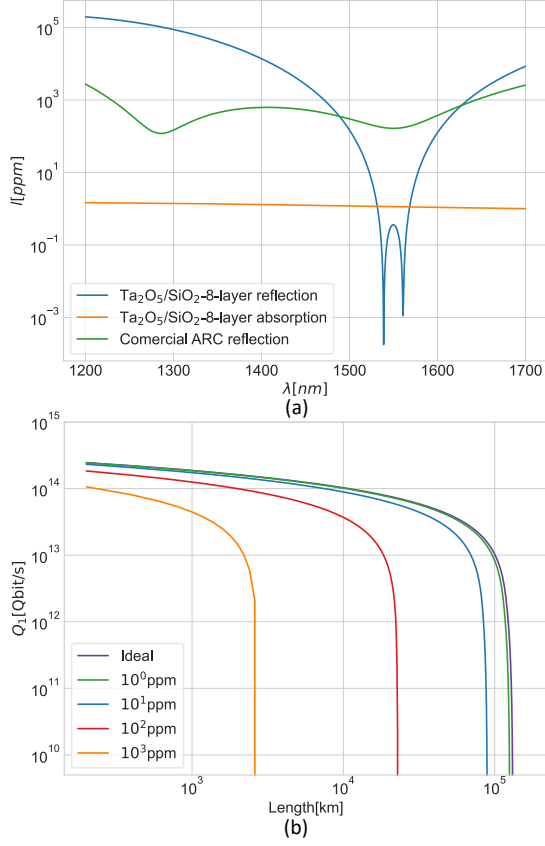


FIG. 4. (a) The estimated reflective loss (blue curve) and material absorption loss (orange curve) of an 8-layer  $\text{Ta}_2\text{O}_5/\text{SiO}_2$  antireflection coating (ARC) on a silica substrate are optimized around 1550 nm. The estimated absorption loss for this design bounds the total loss of ARC above 1 ppm. Additionally, commercially available telecom band ARC loss, with different design parameters (green curve), can already achieve the reflective loss at the 100 ppm level [31]. (b)  $Q_1$  vs distance under losses levels of  $l_{\text{loss}} = 1$  to  $10^3$  ppm with  $L_0 = 4$  km,  $R = 10$  cm,  $\sigma_s = 0.1$  mm, and  $\frac{\sigma_{L_0}}{L_0} = \frac{\sigma_f}{f} = 0.1\%$  at 1 Pascal. The red curve shows that even with a commercial-level ARC loss, it is still possible to achieve sufficient low loss up to  $10^4$  km.

obtain an upper bound for the effective attenuation rate induced by imperfect alignment for parameters deviated from the confocal design as:

$$\alpha_{\text{align}} \leq -\frac{10}{L_0} \log \left[ 1 - \frac{4\pi\sigma_s^2}{\lambda(F^2 + 1)f_{\text{eq}}} - \frac{1}{F^2} \left( \frac{\sigma_f^2}{f^2} + \frac{\sigma_{L_0}^2}{L_0^2} \right) \right], \quad (\text{B6})$$

where  $F = 2f_{\text{eq}}/L_0 \approx 1$ , and  $\sigma_s$  and  $\sigma_{L_0}$  are the magnitudes of the fluctuations of transverse and longitudinal displacements for each lens, and  $\sigma_f$  is the deviation of the focal length.

## Appendix C: Misalignment in VBG

The misalignment will result in the mode conversion and thus cause the loss in the fundamental mode [34]. In this paper, we only consider the misalignment loss due to the displacement of the lens as well as the fluctuation of the focal length of the lens caused by manufacture imperfect. The tilting of lenses has been shown to be the higher-order correction and thus can be neglected [35]. Therefore, the loss in power ratio per section caused by misalignment can be written as a sum as follows when each term is small enough,

$$l_{\text{align}} = l_s + l_f + l_{L_0}, \quad (\text{C1})$$

where  $l_s$ ,  $l_{L_0}$ ,  $l_f$  denote the losses caused by transversal displacement, parallel displacement and the fluctuation of the focal length of the lenses, and only depend on the misalignment parameter  $\sigma_s$ ,  $\sigma_{L_0}$  and  $\sigma_f$  respectively. In general, the loss may not necessarily be a constant for each section due to the power conversion back from higher order mode. However, neglecting such contributions will always give us an upper bound of the loss, which is the practice in this paper.

### 1. Loss caused by parallel displacement

If the field is in perfect fundamental mode while the next lens is shifted for a distance of  $\sigma_{L_0}$ , then the field of the fundamental mode right before the next lens can be simply written as  $E'_b \equiv E_0^0(r, \phi, L_0/2 + \sigma_{L_0})$ . When calculating the loss, we shall expand such field in the basis of the Beam Guide modes  $E_n^m(r, \phi, L_0/2)$ , so that we always keep tracking of the perfect fundamental mode components,  $E_b \equiv E_0^0(r, \phi, L_0/2)$ , emitting at the next lens. And thus the loss is simply given by

$$l_{L_0} \leq 1 - \frac{|\iint E_b E_b'^* r dr d\phi|^2}{|\iint E_b E_b^* r dr d\phi|^2}. \quad (\text{C2})$$

After some routine calculations, we can calculate the upper bound

$$1 - \frac{|\iint E_b E_b'^* r dr d\phi|^2}{|\iint E_b E_b^* r dr d\phi|^2} = \frac{\sigma_{L_0}^2/L_0^2}{F^2 + \sigma_{L_0}^2/L_0^2} \approx \frac{\sigma_D^2/L_0^2}{F^2}. \quad (\text{C3})$$

### 2. Loss caused by imperfect focal length

Now, we suppose that the focal length of the current lens is shifted by  $\sigma_f$ , and such shifting results in a new phase factor of the lens as

$$\exp(i\psi_l) = \exp \left[ -\frac{ik}{2(f + \sigma_f)} r^2 \right]. \quad (\text{C4})$$

Then we plug in the new phase factor and use the inner product method in Section. C1 to derive the loss.



Equivalently, we can adapt the perturbation method [34] in early literature here for a more convenient derivation. The focal length deviation gives rise to an additional phase factor as

$$\exp(i\Delta\psi_f) \approx \exp\left(-\frac{ik}{2f^2}\sigma_f r^2\right) \approx 1 - \frac{ik}{2f^2}\sigma_f r^2 \quad (\text{C5})$$

which slightly converts the fundamental mode into the first-order mode

$$i\Delta\psi_f E_0^0 \rightarrow i\frac{\sigma_f/f}{F} E_1^0, \quad (\text{C6})$$

while the conversion to other modes is higher order in  $\sigma_f/f$ . Therefore, the fraction of excitation loss from the fundamental mode to the first order mode (1, 0) is

$$l_f \leq \left|\frac{i\sigma_f/f}{F}\right|^2 \frac{|\iint E_1^0 E_1^{0*} r dr d\phi|}{|\iint E_b E_b^* r dr d\phi|} = \frac{\sigma_f^2/f^2}{F^2}. \quad (\text{C7})$$

### 3. Loss caused by transversal displacement

For transversal displacement, a naive error model is that assuming there is a “correct” position for each lens determined by geodesic connecting two end-point of VBG, along which each lens’s transversal displacement is fluctuating with variance  $\sigma_s$ . To proceed with the calculation, we use the techniques in Section. C2 to identify the additional phase shift as

$$i\Delta\psi_s = -\frac{ik}{2f}\sigma_s r(e^{i\phi} + e^{-i\phi}). \quad (\text{C8})$$

Repeating the procedure again, we find that

$$i\Delta\psi_s E_0^0 = \sqrt{\frac{k}{(F^2 + 1)f_{eq}}}\sigma_s (E_0^1 + E_0^{-1}), \quad (\text{C9})$$

following which, the loss is

$$l_s \leq \frac{2}{F^2 + 1} \frac{2\pi\sigma_s^2}{\lambda f_{eq}}. \quad (\text{C10})$$

The above error model is widely applied in the early literature discussing the effect of misalignment [11, 34–36], while it requires the ability to identify the “correct” position for each lens over such a large scale system as VBG. In principle, this can be done by scanning the offset of each lens by advanced sensing technique for many times to minimize the error, after which the variance shall be dominated by adjustment precision of the optical bench.

However, a more common practice is that we use the previous lens’s location as reference to align the next lens [37]. In this model, we shall assume that each lens has a random offset of  $\sigma_s$  referred to the location of the previous lens and we always keep tracking of fundamental mode in the coordinate “attached” to each lens instead

of the “correct” position. In this model, one can show that the additional phase is replaced by

$$i\Delta\psi'_s = \left[\frac{2}{w^2(L_0/2)} + \frac{k}{4f}\right]\sigma_s r(e^{i\phi} + e^{-i\phi}). \quad (\text{C11})$$

And thus the loss is calculated as

$$l'_s \leq \frac{1}{2} \frac{2\pi\sigma_s^2}{\lambda f_{eq}}. \quad (\text{C12})$$

we observe that the loss is even smaller by a factor of approximately 2. This can be understood from the aspect of geometrical optics: when the waist of the light is shifted down from the center of the lens, the image of the waist should shift up from the center. And thus the new power center is closer to the reference line of the lens’s center instead of the shifted incident beam center.

Finally, we make a comment on the misalignment parameter we select as default in this paper. 0.1% of relative error of  $D$  and  $f$  will result in an absolute standard deviation of meter level, which shall be able to be easily achieved. In addition, the alignment techniques used by accelerator [38], LIGO [39] and satellite [40] has demonstrated that a standard deviation,  $\sigma_s = 0.1\text{mm}$ , is practically feasible.

### Appendix D: Effective Characteristic Length

As we can see from Eq. 1 and Fig. 2, the performance of VBG is basically limited by the lens loss ( $\alpha_{\text{lens}}$ ) and the alignment loss ( $\alpha_{\text{align}}$ ), because the gas loss ( $\alpha_{\text{gas}}$ ) at telecom-band wavelength can be negligible when we reduce the pressure below 1 Pa.

The transverse displacement is the dominant contribution to the alignment loss, since the achievable longitudinal displacement and focal-length deviations can be sufficiently small ( $\frac{\sigma_{L_0}}{L_0}, \frac{\sigma_f}{f} < 10^{-3}$ ). Hence, according to Eq. 2, we have  $l_{\text{align}} \simeq \frac{2\sigma_s^2}{w_0^2}$ , with transversal displacement  $\sigma_s$ , spacing  $L_0 = 4$  km and beam waist  $w_0 \approx 3$  cm.

To see how these two factors affect the performance of VBG, we define the effective characteristic length  $L_{Q1}$  as the distance at which the one-way quantum capacities of VBG vanishes, i.e.  $\eta = 50\%$  for the corresponding wavelength. We make a 2-D contour plot of characteristic length  $L_{Q1}$  with respect to the lens loss  $\alpha_{\text{lens}}$  (or  $l_{\text{lens}}$  defined in Eq. A2) and transversal displacement  $\sigma_s$ . Using Eq. 1 and Eq. 2, one can approximate the characteristic length as,

$$L_{Q1} = -L_0 \frac{\ln 2}{\ln\left(1 - l_{\text{lens}} - \frac{2\sigma_s^2}{w_0^2} - l_{\text{others}}\right)}, \quad (\text{D1})$$

where  $l_{\text{lens}}$  includes all sources of lens-related loss as listed in Table I and  $l_{\text{others}} \approx 2$  ppm denotes some other losses including parallel perturbation and residue gas absorption.

We plot the characteristic length of VBG under various lens and misalignment configurations in Fig. 2. VBG is quite sensitive to transversal misalignment, in order to have a characteristic length over  $10^4$  km, we must control the transversal misalignment to sub-millimeter level while a total lens loss of a few hundred ppm is sufficient. We also notice that based on the configuration achievable by current techniques with 1 ppm lens loss, VBG has a saturated performance with characteristic length over around  $10^5$  km, which is larger than the perimeter of the earth.

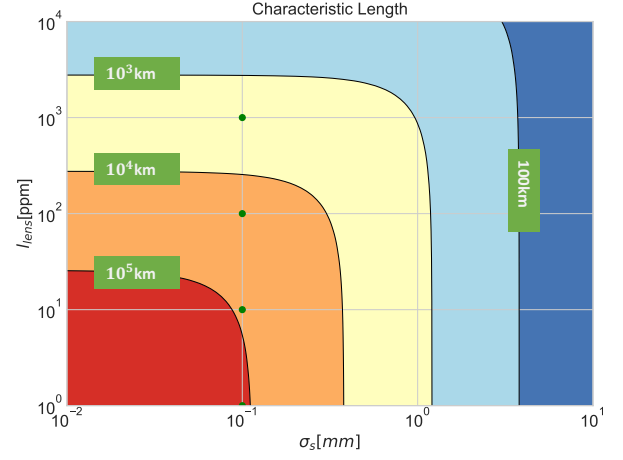


FIG. 5. Characteristic length under various configurations of  $l_{\text{lens}}$  and  $\sigma_s$  with  $L_0 = 4$  km,  $R = 10$  cm, and  $\frac{\sigma_{L_0}}{L_0} = \frac{\sigma_f}{f} = 0.1\%$  at 1 Pascal. The green dots here show the configurations calculated in Fig. 4 (b).